H0LiCOW – I. H_0 Lenses in COSMOGRAIL's Wellspring: program overview

S. H. Suyu,[1,2,3]* V. Bonvin,[4] F. Courbin,[4] C. D. Fassnacht,[5] C. E. Rusu,[5] D. Sluse,[6] T. Treu,[7] K. C. Wong,[2,8] M. W. Auger,[9] X. Ding,[7,10] S. Hilbert,[11,12] P. J. Marshall,[13] N. Rumbaugh,[5] A. Sonnenfeld,[7,14,15] M. Tewes,[16] O. Tihhonova,[4] A. Agnello,[17] R. D. Blandford,[13] G. C.-F. Chen,[2,5] T. Collett,[18] L. V. E. Koopmans,[19] K. Liao,[7] G. Meylan[4] and C. Spiniello[1]

Affiliations are listed at the end of the paper

ABSTRACT

Strong gravitational lens systems with time delays between the multiple images allow measurements of time-delay distances, which are primarily sensitive to the Hubble constant that is key to probing dark energy, neutrino physics and the spatial curvature of the Universe, as well as discovering new physics. We present H0LiCOW (H_0 Lenses in COSMOGRAIL's Wellspring), a program that aims to measure H_0 with <3.5 per cent uncertainty from five lens systems (B1608+656, RXJ1131−1231, HE 0435−1223, WFI2033−4723 and HE 1104−1805). We have been acquiring (1) time delays through COSMOGRAIL and Very Large Array monitoring, (2) high-resolution *Hubble Space Telescope* imaging for the lens mass modelling, (3) wide-field imaging and spectroscopy to characterize the lens environment and (4) moderate-resolution spectroscopy to obtain the stellar velocity dispersion of the lenses for mass modelling. In cosmological models with one-parameter extension to flat Λ cold dark matter, we expect to measure H_0 to <3.5 per cent in most models, spatial curvature Ω_k to 0.004, w to 0.14 and the effective number of neutrino species to 0.2 (1σ uncertainties) when combined with current cosmic microwave background (CMB) experiments. These are, respectively, a factor of ∼15, ∼2 and ∼1.5 tighter than CMB alone. Our data set will further enable us to study the stellar initial mass function of the lens galaxies, and the co-evolution of supermassive black holes and their host galaxies. This program will provide a foundation for extracting cosmological distances from the hundreds of time-delay lenses that are expected to be discovered in current and future surveys.

Key words: gravitational lensing: strong – quasars: individual: B1608+656, RXJ1131−1231, HE 0435−1223, WFI2033−4723, HE 1104−1805 – galaxies: structure – cosmological parameters – distance scale.

1 INTRODUCTION

In the past decade, the so-called flat Λ cold dark matter (ΛCDM) cosmological model consisting of dark energy (with density characterized by a cosmological constant Λ) and CDM in a spatially flat Universe has emerged as the standard cosmological model. This simple model has provided excellent fit to various cosmological observations including the temperature anisotropies in the cosmic microwave background (CMB) and galaxy density correlations in baryon acoustic oscillations (BAO). Recent CMB experiments,

particularly the *Wilkinson Microwave Anisotropy Probe* (*WMAP*; Komatsu et al. 2011; Hinshaw et al. 2013) and the *Planck* satellite (Planck Collaboration XVI 2014; Planck Collaboration XIII 2016), and BAO surveys (e.g. Anderson et al. 2014; Kazin et al. 2014; Ross et al. 2015), have yielded stringent constraints with unprecedented precision on cosmological parameters in the spatially flat ΛCDM model.

An interesting result from *Planck* is its predicted value of the Hubble constant (H_0), a key cosmological parameter that sets the present-day expansion rate as well as the age, size and critical density of the Universe. *Planck* does not directly measure H_0, but rather enables its indirect inference through measurements of combinations of cosmological parameters given assumptions of the
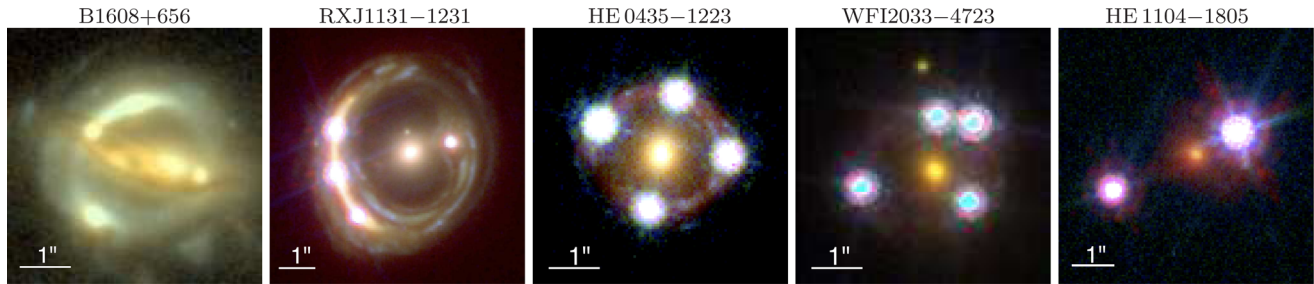
Figure 1. H0LiCOW lens sample, consisting of four quadruply lensed quasar systems in various configurations and one doubly lensed quasar system. The lens name is indicated above each panel. The colour images are composed using two (for B1608+656) or three (for other lenses) *HST* imaging bands in the optical and near-infrared. North is up and east is left.

background cosmological model. Intriguingly, *Planck*'s value of $H_0 = 67.8 \pm 0.9 \, \text{km s}^{-1} \, \text{Mpc}^{-1}$ (Planck Collaboration XIII 2016), from *Planck* temperature data and *Planck* lensing under the flat ΛCDM model, is lower than recent direct measurements based on the distance ladder, of $73.24 \pm 1.74 \, \text{km s}^{-1} \, \text{Mpc}^{-1}$ from the SH0ES program (Riess et al. 2016) and of $74.3 \pm 2.1 \, \text{km s}^{-1} \, \text{Mpc}^{-1}$ (Freedman et al. 2012) from the Carnegie-Chicago Hubble Program (Beaton et al. 2016). On the other hand, *Planck*'s H_0 value is similar to the results of some of the megamaser measurements (e.g. $H_0 = 68.9 \pm 7.1 \, \text{km s}^{-1} \, \text{Mpc}^{-1}$ from Reid et al. 2013, $H_0 = 73^{+26}_{-22} \, \text{km s}^{-1} \, \text{Mpc}^{-1}$ from Kuo et al. 2015 and $H_0 = 66.0 \pm 6.0 \, \text{km s}^{-1} \, \text{Mpc}^{-1}$ from Gao et al. 2016), although the uncertainties of these maser H_0 measurements are still substantial relative to that of *Planck*. A 1 per cent *direct* measurement of the Hubble constant is highly needed: such 1 per cent measurements of H_0 would address the possible tension with the CMB value which, if significant, would point towards deviations from the standard flat ΛCDM and new physics. In fact, when one relaxes, for example, the flatness or Λ assumption in the CMB analysis, strong parameter degeneracies between H_0 and other cosmological parameters appear, and the degenerate H_0 values from the CMB become compatible with the local H_0 measurements from the distance ladder (Freedman et al. 2012; Planck Collaboration XIII 2016; Riess et al. 2016). Thus, a 1 per cent measurement of H_0 is crucial for understanding the nature of dark energy, neutrino physics, the spatial curvature of the Universe and the validity of General Relativity (e.g. Hu 2005; Suyu et al. 2012a; Weinberg et al. 2013). In particular, the dark energy figure of merit of any survey that does not directly measure H_0 improves by ~ 40 per cent if H_0 is known to 1 per cent. Furthermore, independent methods to measure H_0 are necessary to overcome systematic effects, such as the known unknowns (e.g. the effects of crowding or metallicity dependence in the cosmic distance ladder) and the unknown unknowns in order to robustly verify or rule out the standard cosmological paradigm.

Strong gravitational lenses with measured time delays between the multiple images provide a competitive approach to measuring the Hubble constant, completely independent of the local distance ladder: we have demonstrated that we can constrain H_0 to ~ 7–8 per cent precision from a single time-delay lens system with ancillary data (Suyu et al. 2010, 2014). The time-delay method was first proposed by Refsdal (1964) even before the discovery of the first strong gravitational lens system (Walsh, Carswell & Weymann 1979), consisting of a foreground mass distribution that is located close along the line of sight to a background source (see Treu & Marshall 2016, for a recent review). The light from the background source is deflected by the foreground 'lens' mass dis-

tribution; such light bending produces distorted and, in rare cases of 'strong lensing', multiple and often spectacular images of the background source (e.g. Fig. 1).

When the background source is one that varies in its luminosity, such as an active galactic nucleus (AGN; e.g. Vanderriest et al. 1989; Schechter et al. 1997; Fassnacht et al. 1999, 2002; Kochanek et al. 2006; Courbin et al. 2011) or a supernova (SN; e.g. Quimby et al. 2014; Kelly et al. 2015, 2016; Goobar et al. 2016; Grillo et al. 2016; Kawamata et al. 2016; More et al. 2016b; Treu et al. 2016), the variability is manifest in each of the multiple images, but delayed in time relative to each other due to the different light paths. This time delay (Δt) thus depends on the 'time-delay distance' ($D_{\Delta t}$) and the lens mass distribution. Specifically, $\Delta t = D_{\Delta t} \Delta \phi / c$, where $\Delta \phi$ is the Fermat potential difference that is determined by the lens mass distribution and c is the speed of light. Therefore, by measuring the time delay from photometric light curves of the quasar images and modelling the lens mass distribution, one can determine the time-delay distance to the lens system and use the distance–redshift relation to constrain cosmological models.

More precisely, the time-delay distance is

$$D_{\Delta t} \equiv (1 + z_\mathrm{d}) \frac{D_\mathrm{d} D_\mathrm{s}}{D_\mathrm{ds}} \tag{1}$$

(Refsdal 1964; Suyu et al. 2010), where z_d is the redshift of the foreground deflector (also referred to as the strong lens), D_d is the angular diameter distance to the deflector, D_s is the angular diameter distance to the source and D_ds is the angular diameter distance between the deflector and the source. This time-delay distance is for a single strong-lens plane, with other line-of-sight mass distributions only weakly perturbing the strong-lens system and characterized via external shear and convergence. For cases where there are massive line-of-sight mass distributions at a different redshift from the strong-lens galaxy yet close in projection to it such that these massive structures cannot be well approximated by an external shear/convergence, it is necessary to use the multiplane lensing formalism (e.g. Blandford & Narayan 1986; Schneider, Ehlers & Falco 1992). In general, multilens plane ray tracing does not yield a single time-delay distance but rather several combinations of distances. None the less, even in some of these cases, we can derive an effective time-delay distance.

As a result of the unique combination of these three angular diameter distances, the time-delay distance $D_{\Delta t}$ is primarily sensitive to the Hubble constant, in contrast to other non-local distance probes such as SN that probe relative luminosity distances (e.g. Riess et al. 1998; Perlmutter et al. 1999; Conley et al. 2011;

Suzuki et al. 2012; Betoule et al. 2014) and BAO (e.g. Eisenstein et al. 2005; Percival et al. 2010; Blake et al. 2011; Anderson et al. 2014) that yield absolute angular diameter distances. We note though that BAO, together with the CMB, can be used to calibrate the absolute magnitude of SN; assuming that the absolute magnitude of SN does not evolve with redshift, this combination of BAO and SN provides an 'inverse-distance ladder' for the Hubble constant that is insensitive to assumptions on dark energy properties and spatial curvature (e.g. Heavens, Jimenez & Verde 2014; Aubourg et al. 2015). While BAO and the time-delay method both provide angular diameter distance measurements, the distinction is that BAO gives angular diameter distances at specific redshifts whereas the time-delay method yields time-delay distances ($D_{\Delta t}$) which are each a combination of three angular diameter distances. One could in fact determine the angular diameter distance to the lens $D_{\rm d}$ in addition to $D_{\Delta t}$ for time-delay lenses that have stellar velocity dispersion measurements of the foreground lens galaxy (Paraficz & Hjorth 2009; Jee, Komatsu & Suyu 2015). Without time delays, lenses with stellar velocity dispersion measurements can still offer a way to determine the cosmological matter and dark energy density parameters via a ratio of angular diameter distances (e.g. Futamase & Hamana 1999; Futamase & Yoshida 2001; Grillo, Lombardi & Bertin 2008). Recently, Jee et al. (2016) have shown that measurements of $D_{\Delta t}$ and $D_{\rm d}$ from a modest sample of time-delay lenses with lens velocity dispersion measurements yield competitive constraints on cosmological models. In practice, both distances appear as intermediate quantities between the sought after cosmological parameters and the observed quantities.

In order to measure distances precisely and accurately from time-delay lenses, we need four key ingredients in addition to the spectroscopic redshifts of the lens and the source: (1) time delays, (2) high-resolution and high signal-to-noise ratio images of the lens systems, (3) characterization of the lens environment and (4) stellar velocity dispersion of the lens galaxy. These can be obtained via imaging and spectroscopy from *Hubble Space Telescope* (*HST*) and ground-based observatories. In Section 2, we detail each of these requirements.

We initiated the H0LiCOW (H_0 Lenses in COSMOGRAIL's Wellspring) program with the aim of measuring the Hubble constant with better than 3.5 per cent precision and accuracy (in most background cosmological models), through a sample of five time-delay lenses. We obtain the key ingredients to each of the lenses through observational follow-ups and novel analysis techniques. In particular, we have high-quality lensed quasar light curves, primarily obtained via optical monitoring by the COSMOGRAIL (COSmological MOnitoring of GRAvItational Lenses; e.g. Courbin et al. 2005; Vuissoz et al. 2008; Courbin et al. 2011; Tewes et al. 2013b) and Kochanek et al. (2006) teams but also via radio-wavelength monitoring (Fassnacht et al. 2002). COSMOGRAIL has been monitoring more than 20 lensed quasars for more than a decade. The unprecedented quality of the light curves combined with new curve-shifting algorithms (Tewes, Courbin & Meylan 2013a) lead to time delays with typically ~3 per cent accuracy (Fassnacht et al. 2002; Courbin et al. 2011; Tewes et al. 2013b). In addition, we obtain *HST* imaging that reveal the 'Einstein ring' of the lens systems in high resolution, and develop state-of-the-art lens modelling techniques (Suyu et al. 2009; Suyu & Halkola 2010; Suyu et al. 2012b) and kinematic modelling methods (Auger et al. 2010; Sonnenfeld et al. 2012) to obtain the lens mass distribution with a few percent uncertainty (e.g. Suyu et al. 2013, 2014). We further obtain wide-field imaging and spectroscopy to characterize the environment of the field, as well as the spectroscopy of the lens galaxy to obtain the stellar velocity dispersion. The exquisite follow-up data set that we have acquired allow us not only to constrain cosmology but also to study lens galaxy and source properties for understanding galaxy evolution, including the dark matter distribution in galaxies, the stellar initial mass function of galaxies and the co-evolution between supermassive black holes and their host galaxies.

A crucial aspect of our program is the use of blind analysis (e.g. Conley et al. 2006; Suzuki et al. 2012; Suyu et al. 2013; von der Linden et al. 2014) to test for residual systematics and avoid subconscious experimenter bias. In particular, we have developed core analysis techniques for the first lens whose dissection was not blinded (B1608+656; Suyu et al. 2010); we subsequently build upon these techniques and perform blind analysis on the other lenses in the sample. In the blind analysis, the idea is not to blind all the model parameters being inferred, but rather just the cosmological parameters that we aim to measure (as well as any derived parameters or summary statistics from which we could infer the cosmological parameters). We therefore blind the time-delay distance and all cosmological parameters in our analysis. Specifically, throughout the analysis, we only ever plot these blinded parameters offset by their posterior median value. We can then still use the parameter correlations and the uncertainties to cross check our analysis, since the temptation to stop investigating systematic errors when the 'right answer' has been obtained has been removed. Only when the collaboration deems the analysis to be final and complete do we 'open the box' to reveal the median values of the parameters, and then publish these results without modifications.

This paper (hereafter H0LiCOW Paper I) is the first of the series, and gives an overview of the program. There are four more papers that detail the data sets and analysis of the H0LiCOW lens system HE 0435−1223. In particular, Sluse et al. (2017, hereafter H0LiCOW Paper II) present the spectroscopic follow-up of the strong-lens field to measure redshifts of massive and nearby objects close in projection to the strong-lens system and identify galaxy groups along the line of sight. Rusu et al. (2017, hereafter H0LiCOW Paper III) use our multiband wide-field imaging to characterize the lens environment in combination with ray tracing with numerical simulations. Wong et al. (2017, hereafter H0LiCOW Paper IV) perform the lens mass modelling of the strong-lens system incorporating the time delays, high-resolution imaging and lens stellar kinematics data sets to infer the distance to the lens via blind analysis. Bonvin et al. (2017, hereafter H0LiCOW Paper V) present the time-delay measurements from COSMOGRAIL lens monitoring and the cosmological inference based on the previous three papers.

The outline of this paper is as follows. We describe the key ingredients for time-delay cosmography in Section 2, present the five H0LiCOW lens systems in Section 3 and describe our observational campaign in Section 4. The key components of the four analysis papers introduced above are summarized in Section 5. We show the forecasted cosmographic constraints from the H0LiCOW sample in Section 6. We summarize in Section 7 with an outlook for the program.

2 OBSERVATIONAL REQUIREMENTS OF THE TIME-DELAY METHOD

In this section, we describe the observational requirements of the four ingredients for accurate and precise distance measurements from time-delay lenses.

(i) *Time delays*. Monitoring campaigns to map out the variability of the multiple lensed images over time have been carried out both in the radio and optical wavelengths (e.g. Vanderriest et al. 1989; Schechter et al. 1997; Burud et al. 2002; Fassnacht et al. 2002; Hjorth et al. 2002; Kochanek et al. 2006; Vuissoz et al. 2007; Rumbaugh et al. 2015). Regular and frequent observations, at least once every few days, are necessary so that the variability pattern of the background source can be observed in each of the multiple images and be matched up to obtain the time delays. Monitoring in the optical requires a long baseline or high photometric precision to overcome systematic variations due to microlensing by stars in the lensing galaxy that could be mistaken as the background source intrinsic variability (e.g. Tewes et al. 2013b; Sluse & Tewes 2014). Curve-shifting methods have been developed to measure the time delays from the light curves (e.g. Press, Rybicki & Hewitt 1992; Pelt et al. 1996; Fassnacht et al. 2002; Harva & Raychaudhury 2008; Morgan et al. 2008; Hirv, Olspert & Pelt 2011; Hojjati, Kim & Linder 2013; Tewes, Courbin & Meylan 2013a). A recent time-delay challenge showed that some of the methods can recover accurately the time delays in a blind test (Dobler et al. 2015; Liao et al. 2015), particularly the methods we use from the COSMO-GRAIL collaboration (e.g. Tewes et al. 2013a; Bonvin et al. 2016).

(ii) *Well-resolved lensed images*. The strong-lensing information, such as the multiple image positions of the background source, is needed to obtain the foreground lens mass distribution for converting the time delays into distances. Deep and high-resolution imaging of the strong-lens system reveal the 'Einstein rings' that are the spatially extended and lensed images of the background source, such as the host galaxy of the AGN. In the past decade, methods have been developed to take advantage of the thousands of intensity pixels of the extended images to constrain precisely within a few percent the lens potential at the location of the multiple images (e.g. Kochanek, Keeton & McLeod 2001; Warren & Dye 2003; Treu & Koopmans 2004; Koopmans 2005; Dye et al. 2008; Suyu et al. 2009; Vegetti & Koopmans 2009; Suyu et al. 2013; Birrer, Amara & Refregier 2015; Chen et al. 2016). The time-delay distance is particularly sensitive to the radial profile of the lens galaxy mass distribution (e.g. Kochanek 2002; Wucknitz 2002; Wucknitz, Biggs & Browne 2004; Suyu 2012). Imaging with high-signal-to-noise ratio and high angular resolution of the Einstein ring helps to constrain the lens radial profile in the region of the ring, and hence the time-delay distance, up to a mass-sheet transformation (described below).

(iii) *The lens environment*. The distribution of mass external to the lens galaxy, such as that associated with galaxies which are close in projection to the lens system along the line of sight, affects the time delays between the multiple images and hence our cosmological distance measurements. An external convergence κ_{ext} can be absorbed by the lens and source model leaving the fit to the lensed images unchanged, but the predicted time delays altered by a factor of $(1 - \kappa_{ext})$.

To break this 'mass-sheet degeneracy' (MSD; Falco, Gorenstein & Shapiro 1985), one can study the environment of the lens system to constrain κ_{ext} within a few percent[1] through spectroscopic/photometric observations of local galaxy groups and line-of-sight structures (e.g. Fassnacht et al. 2006; Momcheva et al. 2006, 2015) in combination with ray tracing through numerical *N*-body simulations (e.g. Hilbert et al. 2007, 2009; Suyu et al. 2010; Collett et al. 2013; Greene et al. 2013). Furthermore, McCully et al.

(2014, 2016) developed a new framework to model line-of-sight mass distributions efficiently and quantified the environment effects through realistic simulations of lens fields. By reconstructing the three-dimensional mass distribution of strong-lens sightlines, McCully et al. (2016) can obtain constraints on κ_{ext} that are consistent with but tighter than those from the aforementioned statistical approach of combining galaxy number density observations with *N*-body simulations (see also Collett et al. 2013 whose sightline mass reconstruction also produces tighter constraints on κ_{ext} than the statistical approach). Recently, Collett & Cunnington (2016) have pointed out that the external convergence over an ensemble of lenses usually does not average to zero – lenses, like typical massive galaxies, preferentially live in locally overdense regions (Holder & Schechter 2003; Treu et al. 2009; Fassnacht, Koopmans & Wong 2011) and are therefore slightly easier to detect and monitor. None the less, this bias in detection and/or selection that is due to overdensity is expected to have currently negligible impact on $D_{\Delta t}$ (<1 per cent impact). In contrast, measurements of D_d that come from combining delays with the lens velocity dispersion are impervious to κ_{ext} (Jee et al. 2015).

(iv) *The lens galaxy stellar velocity dispersion*. The combination of lensing and stellar kinematics is a powerful probe of the lens galaxy mass distribution (e.g. Romanowsky & Kochanek 1999; Treu & Koopmans 2002; Koopmans et al. 2003; Barnabè et al. 2009, 2011; Sonnenfeld et al. 2012) since the combination breaks degeneracies that are inherent in each approach, and in particular the mass-sheet degeneracy in lensing. Schneider & Sluse (2013) pointed out that the mass-sheet degeneracy can manifest as a lens mass profile degeneracy, which Xu et al. (2016) investigated using simulated galaxies. Moreover, the mass-sheet degeneracy is in fact a special case of a more general 'source-position transformation' (Schneider & Sluse 2014; Unruh, Schneider & Sluse 2016), although this latter transformation typically does not leave the multiple time delays invariant. To break such lensing degeneracies, information from the lens galaxy stellar kinematics is crucial: Suyu et al. (2014) showed that the lens velocity dispersion substantially reduced the dependence of the time-delay distance on lens mass profile assumptions. The lens velocity dispersion is also a key ingredient for measuring D_d, which is more sensitive to dark energy properties than $D_{\Delta t}$ (Jee et al. 2015, 2016).

3 H0LICOW SAMPLE OF LENSES

In Fig. 1, we show the images of the five lenses in our sample. The left four lenses are quadruply lensed quasar systems (quads) and the rightmost lens system is a doubly lensed quasar system (double). As described below, the four quads span the three generic multiple image configurations we have in galaxy-scale strong lenses: symmetric, fold (with two merging images) and cusp (with three merging images). Therefore, our sample will allow us to explore to some extent the optimal image configuration for cosmographic studies.

Our sample of lenses was chosen based on three criteria: (1) availability of accurate and precise time delays, (2) existing measurements of spectroscopic redshifts for both the lens and the background source and (3) the lens system is not located near a galaxy cluster (to avoid potentially large systematic effects due to mass along the line of sight). We prefer quads to doubles since quads provide more observational constraints on the mass model (e.g. more time delays and image positions). The four quads in our sample were the only known quad lenses that passed the above three criteria at the time of our sample selection. There were a few doubles

---

[1] In terms of its impact on $D_{\Delta t}$.

that pass these criteria, and we chose HE 1104−1805 as the first double in this pilot program given its relative simplicity for mass modelling with only one strong-lens galaxy (in contrast to other systems that have multiple massive lens galaxies). We describe in more detail each of the lenses below.

B1608+656. The lens system was discovered in the Cosmic Lens All-Sky Survey (Myers et al. 1995; Browne et al. 2003; Myers et al. 2003). The radio-loud AGN is lensed into four images that are relatively dim in the optical wavelength, thus showing clearly the extended Einstein ring of the AGN host galaxy in the *HST* imaging (Fig. 1). Two of the four multiple images are close together, making this a standard 'fold' configuration. The system contains two lens galaxies that appear to be interacting and resulting in dust extinction in the system (e.g. Koopmans et al. 2003; Surpi & Blandford 2003; Suyu et al. 2009). The lens and source redshifts are, respectively, $z_s = 1.394$ (Fassnacht et al. 1996) and $z_d = 0.6304$ (Myers et al. 1995). This system was the first quad lens with all three time delays measured with uncertainties of only a few percent (Fassnacht et al. 1999, 2002).

RXJ1131−1231. Sluse et al. (2003) discovered RXJ1131−1231 serendipitously during polarimetric imaging of a sample of radio quasars. This system shows a spectacular Einstein ring, with multiple arclets that are the lensed images of the AGN host galaxy containing a bulge and a disk with spiral arms and star formation clumps. Three of the four quasar images are close to each other, forming the typical 'cusp' configuration. The lens redshift is at $z_d = 0.295$ (Sluse et al. 2003, 2007), and the source redshift is at $z_s = 0.654$ (Sluse et al. 2007).[2]

HE 0435−1223. This lens system was found by Wisotzki et al. (2002), originally selected in the Hamburg/ESO survey (Wisotzki et al. 2000) as a highly probable quasar candidate. The background quasar is lensed into four multiple images that are nearly symmetrically positioned in the 'cross' configuration. The background source is at redshift $z_s = 1.693$ (Sluse et al. 2012)[3] and the foreground strong lens is at redshift $z_d = 0.4546$ (Morgan et al. 2005; Eigenbrod et al. 2006). The *HST* image reveals an elliptical ring that connects the four images of the AGN. This ring is produced by the extended lensed images of the AGN galaxy.

WFI2033−4723. Morgan et al. (2004) discovered this quad lens system as part of an optical imaging survey using the MPG/ESO 2.2-m telescope at La Silla, Chile that is operated by the European Southern Observatory (ESO). The lens system exhibits a typical fold configuration, since it contains two merging quasar images. The quasar is at redshift $z_s = 1.662$ (Sluse et al. 2012), which is consistent with the first measurement by Morgan et al. (2004). The quasar images are substantially brighter than the background quasar host galaxy and the foreground lens galaxy. Morgan et al. (2004) identified the foreground lens galaxy, whose redshift was measured to be $z_d = 0.661$ (Eigenbrod et al. 2006), consistent with an earlier measurement by Ofek et al. (2006). The high-resolution *HST* imaging shows several galaxies in the vicinity of the lens system.

---

[2] The source redshift of $z_s = 0.654$ is based on the narrow emission lines, which is considered more accurate than the H α and Mg II lines (Hewett & Wild 2010) that yield $z_s = 0.657$ (Sluse et al. 2007). We note that a 0.003 change in z_s corresponds to a <0.4 per cent change in $D_{\Delta t}$ for RXJ1131−1231, and even less change in $D_{\Delta t}$ for the other higher redshift lens systems.

[3] Based on Mg II emission line, which results in a slightly higher redshift value than the previous measurement of $z_s = 1.689$ (Wisotzki et al. 2002) from C IV line that is known to be prone to systematic blueshifts in many quasars.

Since these galaxies would likely influence the lens potential, their redshifts will be obtained with our ancillary data (Section 4.3) in order to incorporate them into the lens mass model.

HE 1104−1805. This system was also discovered in the early phase of the Hamburg/ESO survey by Wisotzki et al. (1993). The two lensed quasar images are separated by ∼3″ and is unusual in having the brighter image as the one closer to the foreground lens galaxy, which was first identified by Courbin, Lidman & Magain (1998) and Remy et al. (1998). The source is at $z_s = 2.316$ (Smette et al. 1995), and the lens is at a relatively high redshift of $z_d = 0.729$ (Lidman et al. 2000). The *HST* image shows multiple luminous structures/galaxies around the lens system.

4 OBSERVATIONAL FOLLOW-UP

In collaboration with the COSMOGRAIL team, we carry out an observational campaign in order to obtain each of the four ingredients for distance measurements of the H0LiCOW lenses. We describe the monitoring in Section 4.1 to get the time delays, deep *HST* imaging to constrain the lens galaxy mass distribution in Section 4.2, wide-field spectroscopy and imaging to study the lens environment in Section 4.3 and spectroscopy of the foreground lens galaxy to measure the stellar velocity dispersion in Section 4.4.

4.1 Time delays

Of the five H0LiCOW lenses, B1608+656 has been monitored previously by Fassnacht et al. (1999, 2002) using the Very Large Array, whereas the other four lenses are currently being monitored by the COSMOGRAIL and Kochanek et al. (2006) collaborations using a network of 1–2 m optical telescopes, particularly the Euler telescope in Chile.

Using three seasons of monitoring of B1608+656, especially the third season that showed significant variability that repeated in all four quasar images, Fassnacht et al. (2002) measured all three relative time delays between the four quasar images with uncertainties of a few percent. The image fluxes were measured every 3–4 d during the monitoring. The time delays span ∼30–80 d, relative to the first image that varies.

The monitoring of RXJ1131−1231, HE 0435−1223, WFI2033−4723 and HE 1104−1805 by the COSMOGRAIL and Kochanek et al. (2006) teams started in 2003, with a photometric point every 2–4 d. The MCS deconvolution method (Magain, Courbin & Sohy 1998; Cantale et al. 2016) is used to extract the photometry of the quasar images for building the light curves. Tewes et al. (2013a) set up an automated pipeline to reduce the images, build the light curves and measure the time delays using a state-of-the-art curve-shifting algorithm that simultaneously models both intrinsic variability of the AGNs and microlensing variations. With this pipeline, Bonvin et al. (2016) recovered the time delays with a precision of ∼3 per cent and negligible bias for simulated light curves mimicking COSMOGRAIL monitoring in the blind strong-lens time delay challenge (Liao et al. 2015), demonstrating the robustness of their curve-shifting algorithms.

The monitoring and analysis yield time delays in RXJ1131−1231 with a 1.5 per cent uncertainty on the longest delay (Tewes et al. 2013b). The light curve has been separately modelled by A. Hojjati and E. Linder using the Gaussian process technique (Hojjati et al. 2013), who have obtained delays that are consistent with the measurements of Tewes et al. (2013b) (Linder, private communication). The monitoring and analysis of HE 0435−1223 are described

in H0LiCOW Paper V, with a relative uncertainty of 6.5 per cent on the longest delay (between images A and D). The measurement precision in the delays has improved by a factor of 2 compared to the previous measurements by Courbin et al. (2011) with the five additional years of monitoring and improvements in the curve-shifting algorithms. For WFI2033−4723 and HE 1104−1805, we expect to improve on the previous delay measurements by Vuissoz et al. (2008) and Poindexter et al. (2007), respectively, with the new curve-shifting techniques, and estimate relative uncertainties of ∼4 per cent and ∼2 per cent, respectively, from the monitoring campaign.

4.2 *HST* observations

Deep *HST* Advanced Camera for Surveys (ACS) observations of B1608+656 were obtained in Program 10158 (PI: C. D. Fassnacht) in two filters, *F*606*W* and *F*814*W*. Suyu et al. (2009) have described these observations in detail. Furthermore, Suyu et al. (2009) analysed these data and used a pixelated lens potential reconstruction technique to model the lens mass distribution, which were subsequently used for cosmographic analysis in Suyu et al. (2010).

Archival *HST* ACS observations of RXJ1131−1231 (Program 9744; PI: C. S. Kochanek) are available in two filters, *F*555*W* and *F*814*W*. Details of the observations are described in, e.g. Claeskens et al. (2006). These have been used to model the lens mass distribution for cosmography, accounting for uncertainties due to assumptions on the lens mass profile (Suyu et al. 2013, 2014). Recently, Birrer, Amara & Refregier (2016) have also used these observations to model independently the lens mass distribution of RXJ1131−1231 for cosmography, obtaining results that are consistent with Suyu et al. (2013).

We have obtained new deep *HST* Wide Field Camera 3 (WFC3) observations in Program 12889 (PI: S. H. Suyu) of the remaining three lenses (HE 0435−1223, WFI2033−4723 and HE 1104−1805) in the infrared (IR) channel. The goal of these observations is to detect the Einstein rings of the AGN host galaxies at high signal-to-noise ratios, in order to constrain the foreground lens mass distribution (previous *HST* observations had insufficient signal-to-noise ratios of the rings for our analysis). We use the *F*160*W* filter to optimize the contrast between the AGN host galaxy and the AGN, since the host galaxy is brighter in the IR compared to the optical, especially for HE 1104−1805 where the quasar is at a high redshift.

We employ four-point dither patterns that trace out parallelograms with the lengths of the sides being non-integral numbers of pixels. For each lens, we use multiple parallelograms that are offset by non-integral pixels. Specifically, we use 2, 5 and 3 parallelograms for HE 0435−1223, WFI2033−4723 and HE 1104−1805, respectively, depending on the total exposure time needed to image the Einstein ring. We further ensure that the dithering points do not overlap to avoid IR persistence effects. This dithering strategy allows us to recover effectively an angular resolution of ∼0.08 arcsec from the native 0.13 arcsec pixel scale.

Since the AGN host galaxy is substantially fainter than the AGN, we further adopt an exposure sequence of short–long–long at each of the dithering point.[4] The first short exposure allows us to char-

Table 1. New *HST* WFC3/IR Observations of HE 0435−1223, WFI2033−4723 and HE 1104−1805.

Lens	Date	Number/type of exposures	Time (s) per exposure
HE 0435−1223	2012-10-28	8 short exp.	44
		15 long exp.[4]	599
WFI2033−4723	2013-05-03	20 short exp.	74
	to 2013-05-04	4 long exp.[4]	599
		32 long exp.[4]	699
HE 1104−1805	2013-03-18	12 short exp.	26
		24 long exp.	599

Notes. At each dither position, an exposure sequence of short–long–long exposure times is adopted in order to sample the large dynamical range of the AGN and its much fainter host galaxy.[4]

acterize the AGN, whereas the long exposures would get the AGN host with possibly the pixels near the bright AGN saturated. We note that there are multiple non-destructive reads during each exposure with the MULTIACCUM mode of the WFC3/IR detector, so we can have a count rate estimate on the AGN pixels even in the long exposures if several non-destructive reads are available before saturation. The short exposures are taken to ensure that there are sufficient reads to characterize accurately the pixel count rates near the AGN positions, in case the long exposures are indeed saturated with insufficient non-destructive reads. In essence, the combination of the short and long exposures allows us to reconstruct in full the brightness distribution of *both* the lensed AGN and the lensed host galaxy. We summarize our observations in Table 1.

We reduce the images using DRIZZLEPAC.[5] The images are drizzled to a final pixel scale of 0.08 arcsec, without masking the bright AGN pixels as they are well characterized by the short exposures. The uncertainty on the flux in each pixel is estimated from the science image and the drizzled exposure time map by adding in quadrature the Poisson noise from the source and the background noise due to the sky and detector readout.

In Fig. 2, we show the reduced *HST* WFC3 observations of HE 0435−1223, WFI2033−4723 and HE 0435−1223 in the top panels from left to right. In the bottom, we show the images with the lens light subtracted with GLEE,[6] revealing the Einstein ring of the AGN host galaxy. In H0LiCOW Paper IV, we detail the modelling of HE 0435−1223 using multilens-plane ray tracing (e.g. Blandford & Narayan 1986; Schneider et al. 1992; Blandford & Kochanek 2004) and point spread function (PSF) reconstruction techniques developed by Suyu et al. (in preparation). The subtraction of lens light in WFI2033−4723 and HE 1104−1805 (bottom-middle and bottom-right panels of Fig. 2, respectively) is based on an initial PSF built from stars in the field without any lens mass modelling or iterative PSF reconstruction, hence the lens-subtraction residuals. Furthermore, the lens galaxy of HE 1104−1805 is on a diffraction spike of the brighter AGN image – an accurate PSF model would be crucial for distinguishing the lens galaxy, the two AGN images and the lensed host galaxy of the AGN. The full modelling and

---

[4] For HE 0435−1223, one long exposure was lost due to a satellite passing over the target. For one of the parallelogram dither pattern for WFI2033−4723, we use an exposure seq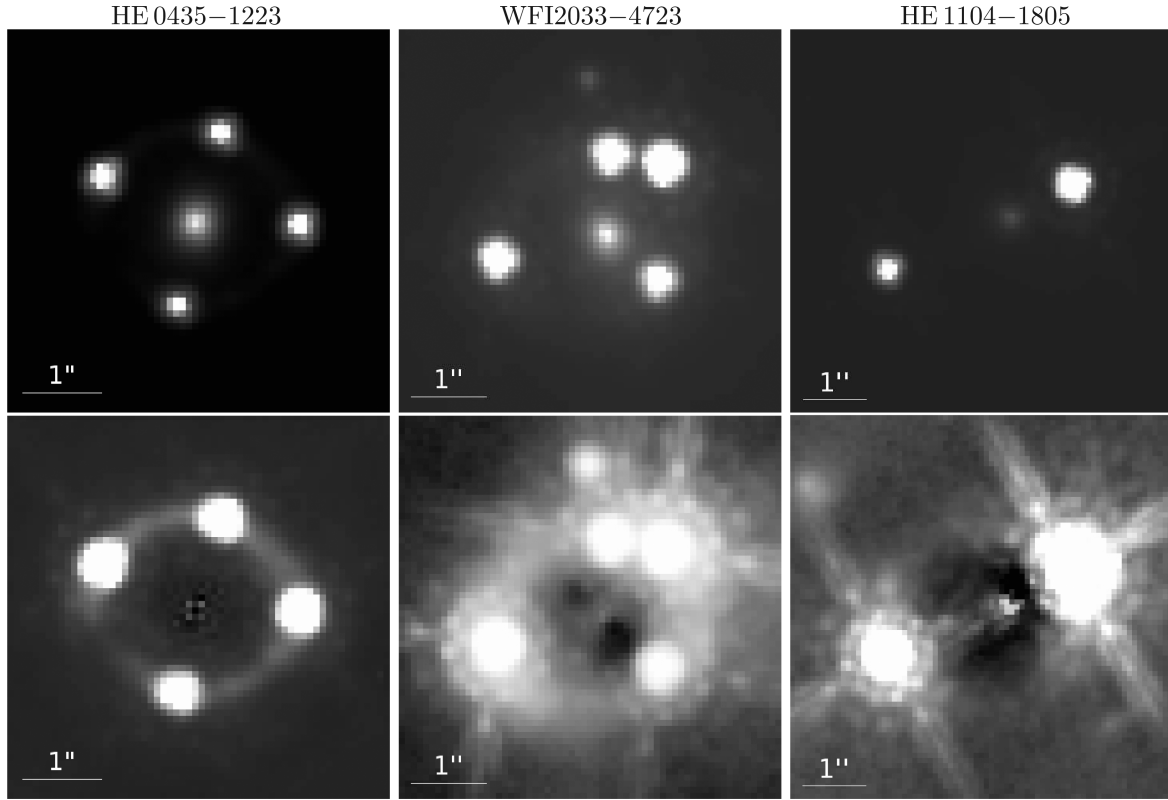uence of short–long (rather than short–long–long) at each dither position to optimize target exposure time given overhead associated with observations.

[5] DRIZZLEPAC is a product of the Space Telescope Science Institute, which is operated by AURA for NASA.

[6] A lens modelling software package developed by A. Halkola and S. H. Suyu (Suyu & Halkola 2010; Suyu et al. 2012b).

Figure 2. *HST* WFC3 *F*160*W* observation of HE 0435−1223, WFI2033−4723 and HE 1104−1805 from left to right in the top panels. In the bottom panels, the lens-galaxy light has been subtracted, revealing the Einstein ring of the AGN host galaxy that is needed for accurate and precise lens mass modelling. The full modelling of HE 0435−1223 is detailed in H0LiCOW Paper IV. The lens subtraction for WFI2033−4723 and HE 1104−1805 in the bottom-middle and bottom-right panels, respectively, is based on an initial PSF model without PSF reconstruction (which we defer to future work), hence the visible residuals. In each of the panels, north is up and east is left.

analysis of WFI2033−4723 and HE 1104−1805 will appear in future publications.

4.3 Wide-field spectroscopy and imaging of lens environment

We obtain wide-field spectroscopy to pinpoint the redshifts of the bright galaxies in the fields of the H0LiCOW lenses, particularly the ones close to the strong lens. Redshifts of nearby galaxies, especially those within a few arcseconds from the strong lens, are crucial since the external convergence approximation is often insufficient for these galaxies (e.g. McCully et al. 2014) and they need to be incorporated directly into the strong-lens modelling. We use the multiobject spectrographs on the Very Large Telescope, the Gemini Telescope and the W. M. Keck Telescope to target our lens fields, as summarized in Table 2. The spectroscopic redshifts and galaxy group identifications are detailed in Fassnacht et al. (2006), H0LiCOW Paper II, and forthcoming publications.

To further characterize the lens environment and determine κ_{ext}, we obtain wide-field multiband imaging using the Canada–France–Hawaii Telescope, Subaru Telescope, the Very Large Telescope, Gemini Telescope and *Spitzer Space Telescope*. Table 3 summarizes the follow-up imaging that allow us to compute the photometric redshifts of structures along the line of sight as well as to estimate their stellar masses. Details of the observations and inference on κ_{ext} are described in H0LiCOW Paper III and forthcoming publications.

Williams et al. (2006) have independently obtained *I* and either *V* or *R* images of all five H0LiCOW lenses using the 4-m Cerro Tololo Inter-American Observatory (CTIO) Blanco telescope for

Table 2. Wide-field spectroscopy of H0LiCOW lenses as part of the H0LiCOW program.

Lens	Facility/instrument	Proposal PI
B1608+656	W. M. Keck/LRIS	C. D. Fassnacht
	W. M. Keck/ESI	C. D. Fassnacht
RXJ1131−1231	W. M. Keck/LRIS	C. D. Fassnacht
HE 0435−1223	W. M. Keck/LRIS	C. D. Fassnacht
	VLT/FORS2	D. Sluse
	Gemini/GMOS	T. Treu
WFI2033−4723	VLT/FORS2	D. Sluse
	Gemini/GMOS	T. Treu
HE 1104−1805	VLT/FORS2	D. Sluse
	Gemini/GMOS	T. Treu

Notes. Abbreviations are LRIS (Low-Resolution Imaging Spectrometer; Oke et al. 1995; Rockosi et al. 2010), ESI (Echellete Spectrograph and Imager; Sheinis et al. 2002), VLT (Very Large Telescope), FORS2 (FOcal Reducer and low dispersion Spectrograph; Appenzeller et al. 1998) and GMOS (Gemini Multi-Object Spectrographs; Hook et al. 2004). Details of the observations for B1608+656 are in Fassnacht et al. (2006), and for the other four lenses are in H0LiCOW Paper II and forthcoming publications. Additional integral field spectroscopy of the central 30 arcmin around WFI2033−4723 has been recently obtained with the Multi Unit Spectroscopic Explorer (MUSE; Bacon et al. 2012) on the VLT.

the southern fields and the 4-m Kitt Peak National Observatory Mayall telescope for the northern fields. Using these images to select spectroscopic targets, Momcheva et al. (2015) have obtained spectroscopic observations of the five H0LiCOW lenses using the

Table 3. Wide-field imaging obtained as part of the H0LiCOW program.

Lens	Facility/instrument	Wavelength bands	Proposal PI
B1608+656	CFHT/MegaCam	u	S. H. Suyu
	Subaru/Suprime-Cam	g, r, i	C. D. Fassnacht
	Subaru/MOIRCS	J, H, K_s	C. D. Fassnacht
	Gemini/NIRI	J, K_s	C. D. Fassnacht
	Spitzer/IRAC	3.6 μm, 4.5 μm	C. E. Rusu
RXJ1131−1231	CFHT/MegaCam	u	S. H. Suyu
	Subaru/Suprime-Cam	g, r, i	C. D. Fassnacht
	Subaru/MOIRCS	J, H, K_s	C. D. Fassnacht
	Gemini/NIRI	J, K_s	C. D. Fassnacht
HE 0435−1223	CFHT/MegaCam	u	S. H. Suyu
	Subaru/Suprime-Cam	g, r, i	C. D. Fassnacht
	Subaru/MOIRCS	H	C. D. Fassnacht
	Gemini/NIRI	J, K_s	C. D. Fassnacht
WFI2033−4723	CTIO Blanco/DECam	u	C. E. Rusu
	VLT/HAWK-I	J, H, K	C. D. Fassnacht
HE 1104−1805	CFHT/MegaCam	u	S. H. Suyu
	Subaru/Suprime-Cam	g, r, i	C. D. Fassnacht
	Subaru/MOIRCS	J, H, K_s	C. D. Fassnacht
	Gemini/NIRI	J, K_s	C. D. Fassnacht

Notes. Abbreviations and references for the instruments are CFHT (Canada–France–Hawaii Telescope) MegaCam (Boulade et al. 2003), Suprime-Cam (Miyazaki et al. 2002), MOIRCS (Multi-Object InfraRed Camera and Spectrograph; Suzuki et al. 2008; Ichikawa et al. 2006), NIRI (Near InfraRed Imager and Spectrometer; Hodapp et al. 2003), IRAC (Infrared Array Camera; Fazio et al. 2004), CTIO (Cerro Tololo Inter-American Observatory) DECam (Dark Energy Camera; Diehl & Dark Energy Survey Collaboration 2012), VLT (Very Large Telescope) HAWK-I (High Acuity Wide field K-band Imager; Pirard et al. 2004; Casali et al. 2006; Kissler-Patig et al. 2008). Details of the observations are in H0LiCOW Paper III and forthcoming publications. WFI2033−4723 is in the footprint of the Dark Energy Survey with observations in g, r, i, z and Y bands, so we did not target WFI2033−4723 in these bands. We observed only B1608+656 with *Spitzer* since the other four lenses have archival *Spitzer*/IRAC observations (PI: C. S. Kochanek).

6.5-m Magellan telescopes. In H0LiCOW Paper II, we merge the spectroscopic catalogue from the multiple spectroscopic campaigns on HE 0435−1223.

4.4 Lens galaxy spectroscopy for lens velocity dispersion

For B1608+656 and RXJ1131−1231, we have obtained long-slit spectra of the lens systems with the Low-Resolution Imaging Spectrometer (LRIS; Oke et al. 1995) at the Keck Observatory for measuring the lens stellar velocity dispersion (Suyu et al. 2010, 2013). For HE 0435−1223, we observe the lens system with LRIS in multiobject mode to obtain spectra of the foreground lens galaxy for lens velocity dispersion measurement (see H0LiCOW Paper IV) and also of nearby galaxies (see H0LiCOW Paper II). Both WFI2033−4723 and HE 1104−1805 have bright AGNs relative to the lens galaxy, making the lens velocity dispersion measurement challenging. We have new observations of WFI2033−4723 with MUSE (Bacon et al. 2012) at the VLT, which we expect will allow us to reduce the uncertainty on the current lens velocity dispersion by a factor of 2, to ∼5–7 per cent precision. The velocity dispersion is a key ingredient to break the MSD/lensing degeneracies (e.g. Suyu et al. 2014). For HE 1104−1805, we obtained one-sixth of our proposed observations with XSHOOTER on the VLT in priority B, which is not sufficient to measure the velocity dispersion. We have time on OSIRIS (OH-Suppressing Infra-Red Imaging Spectrograph; Larkin et al. 2006) on Keck to observe HE 1104−1805, RXJ1131−1231and HE 0435−1223 with adaptive optics. Because OSIRIS is an integral field spectrograph, these observations have the goal of obtaining two-dimensional kinematic data of the foreground lens, which will then be used to further constrain the lens mass models. We summarize the spectroscopic observations for lens velocity dispersion measurement in Table 4.

Table 4. Spectroscopy of foreground lens as part of the H0LiCOW program.

Lens	Facility/instrument	Proposal PI
B1608+656	W. M. Keck/LRIS	C. D. Fassnacht
RXJ1131−1231	W. M. Keck/LRIS	C. D. Fassnacht
	W. M. Keck/OSIRIS	T. Treu
HE 0435−1223	W. M. Keck/LRIS	C. D. Fassnacht
	W. M. Keck/OSIRIS	T. Treu
WFI2033−4723	VLT/MUSE	D. Sluse
HE 1104−1805	VLT/X-shooter	C. Spiniello
	W. M. Keck/OSIRIS	T. Treu

Notes. OSIRIS is the OH-Suppressing Infra-Red Imaging Spectrograph (Larkin et al. 2006). Details of the LRIS observations for B1608+656 are in Suyu et al. (2010), for RXJ1131−1231 are in Suyu et al. (2013), and for HE 0435−1223 are in H0LiCOW Paper IV; other observations are in forthcoming publications. Only one-sixth of the HE 1104−1805 observations with X-shooter (Vernet et al. 2011) were obtained, which were insufficient for measuring the lens velocity dispersion. The observations with OSIRIS are pending.

5 COSMOGRAPHY AND ASTROPHYSICS WITH HE 0435−1223: KEY COMPONENTS

We summarize the key ingredients and analysis of HE 0435−1223 that are described in upcoming publications of the H0LiCOW project (H0LiCOW Papers II–V). The titles of the papers begin with 'H0LiCOW', followed by the specific titles written below.

II. Spectroscopic survey and galaxy-group identification of the strong gravitational lens systems HE 0435−1223 (H0LiCOW Paper II). From our spectroscopic campaign of the lens environment, we present the measured spectroscopic redshifts, focusing in

particular on the massive and nearby objects to the strong-lens system that are necessary ingredients for lens mass modelling and distance measurement. By combining with the spectroscopic catalogue of independent efforts (Momcheva et al. 2015), we identify potential galaxy groups towards HE 0435−1223 in order to control the systematic effect due to the galaxies along the line of sight. We use the flexion shift[7] introduced by McCully et al. (2016) to determine which mass structures (galaxies/groups) need to be incorporated explicitly in the lens mass model and which could be well approximated by an external shear/convergence field. The flexion-shift analysis presented in H0LiCOW Paper II shows that the most significant line-of-sight perturber is the galaxy G1 that is closest to the lens system, which justifies our inclusion of this particular galaxy in all of our strong-lensing models in H0LiCOW Paper IV. Furthermore, the next four nearest perturbers from the lens system may also produce higher order perturbations on the lens potential, and we account for the effects of these four additional galaxies in one of our systematic tests in H0LiCOW Paper IV.

III. Quantifying the effect of mass along the line of sight to the gravitational lens HE 0435−1223 through weighted galaxy counts (H0LiCOW Paper III). Using the wide-field photometry and spectroscopy in Section 4.3, we compute photometric redshifts and stellar masses for objects in the field up to 120 arcsec from the strong lens, and with $i < 24$ mag. We thoroughly test the weighted galaxy number counts technique of Greene et al. (2013), and apply it to HE 0435−1223 with the CFHTLenS survey (Heymans et al. 2012) as the control field. By comparing the weighted counts to simulated lines of sight that are ray traced through numerical simulations (Hilbert et al. 2007, 2009), we infer the distribution for the external convergence κ_{ext} that excludes the strong-lens redshift plane.

IV. Lens mass model of HE 0435−1223 and blind measurement of its time-delay distance for cosmology (H0LiCOW Paper IV). Using the time delays from H0LiCOW Paper V and our *HST*/WFC3-IR imaging (*F160W*) and archival *HST*/ACS observations (*F555W* and *F814W*), we model the lens mass distribution including explicitly the nearest, in projection from HE 0435−1223, one (G1) or five (G1 plus the next four nearest/brightest) perturbers, with spectroscopic redshifts from H0LiCOW Paper II. We then incorporate the velocity dispersion of the lens galaxy, and the external convergence distribution from H0LiCOW Paper III to infer an effective time-delay distance, which is blinded during the analysis stage. We unblind only after the completion of the analysis, and publish these results without modifications.

V. New COSMOGRAIL time delays of HE 0435−1223: H_0 to 3.8 per cent from strong lensing in flat-ΛCDM (H0LiCOW Paper V). We present the 13-yr monitoring of HE 0435−1223 and measure the time delays between the image pairs. Using the resulting effective time-delay distance of HE 0435−1223 from the blind analysis in H0LiCOW Paper IV, we create a Time Delay Strong Lensing (TDSL) probe with HE 0435−1223, RXJ1131−1231 and B1608+656 (we note that the analysis of RXJ1131−1231 was also blinded in Suyu et al. (2013), whereas the analysis of B1608+656

was not as it was the first lens to be analysed using our modelling techniques). We infer cosmological constraints from TDSL alone, and combine it with other cosmological probes to constrain various cosmological models.

In addition to the above, there are more forthcoming publications. The study of the AGN host galaxy properties based on simulations are described in H0LiCOW Paper VI (Ding et al. 2017). The newly developed multilens plane modelling, based on the multilens plane equations (Schneider et al. 1992; Blandford & Kochanek 2004), and PSF reconstruction will be detailed by Suyu et al. (in preparation). The weak-lensing analysis of the field of HE 0435−1223 will be presented by Tihhonova et al. (in preparation). Following these publications, there will be the next studies and analysis of the remaining sample (WFI2033−4723 and HE 1104−1805).

6 H0LICOW COSMOGRAPHIC FORECAST

We make predictions of the cosmographic constraints based on our sample of H0LiCOW lenses. We use the time-delay distance measurements for B1608+656 (equation 35 of Suyu et al. 2010), RXJ1131−1231 (equation 5 of Suyu et al. 2014) and HE 0435−1223 (equation 17 of H0LiCOW Paper IV). For the forecasted time-delay distance measurements of the other two lenses, we adopt an uncertainty with contributions from the time delays, mass modelling and external convergence added in quadrature. Specifically, we estimate time-delay uncertainties of 4 per cent and 2 per cent, modelling uncertainties of 4 per cent and 8 per cent, external convergence uncertainties of 4 per cent and 4 per cent, yielding a total uncertainty of 7 per cent and 9 per cent for WFI2033−4723 and HE 1104−1805, respectively. Furthermore, we assume that the angular diameter distance to each lens can be measured with an uncertainty of 15 per cent using our current data sets (Jee et al. 2015). More precise measurements of D_{d} ($\sim$5–10 per cent uncertainty) would require additional kinematic data of the lens galaxy beyond what we currently have, particularly spatially resolved kinematics maps. For the forecasted $D_{\Delta t}$ and D_{d} constraints, we adopt a fiducial cosmological model with $H_0 = 72\,\mathrm{km\,s^{-1}\,Mpc^{-1}}$, $\Omega_{\mathrm{m}} = 1 - \Omega_{\mathrm{DE}} = 0.32$, and $w = -1$ to predict the distances with their estimated uncertainties mentioned above, although we note that this assumption affects little the fractional uncertainty, which is nearly scale-free.

We show in Fig. 3, the cosmographic constraints of our sample of lenses with uniform priors on the cosmological parameters (left-column panels), in combination with *WMAP* 9-yr results (Hinshaw et al. 2013, middle-left-column panels), and in combination with *Planck* 2015 results (Planck Collaboration XIII 2016, middle-right-column panels)[8] for three different background cosmologies: (1) open ΛCDM with variable spatial curvature Ω_{k} (top row), (2) spatially flat wCDM with w as the time-independent dark energy equation of state (middle row) and (3) flat ΛCDM with varying effective number of relativistic species N_{eff} (bottom row). In the right-column panels, we show the one-dimensional marginalized constraints of H_0 of our sample of lenses alone or in combination with the CMB data sets (i.e. marginalized H_0 distributions of the panels to the left), as indicated in the legend. We list in Table 5 the prior ranges for the uniform background cosmologies. The *WMAP* 9-yr and *Planck*

---

[7] The flexion shift corresponds to the shift in the image positions due to the flexion (third-order derivatives of the lens potential) of a line-of-sight perturber. McCully et al. (2016) find through their study of simulated lens fields that perturbers with flexion shifts larger than $\sim$10^{-4} arcsec should be incorporated explicitly in the multiplane lens mass model. The threshold of $\sim$10^{-4} arcsec is conservative and is based on tests that only used image positions as constraints. It may be that using the spatially extended images for modelling would push that threshold even lower.

[8] We use the *Planck* chains designated by 'plikHM_TT_lowTEB' that uses the baseline high-L *Planck* power spectra and low-L temperature and LFI polarization.
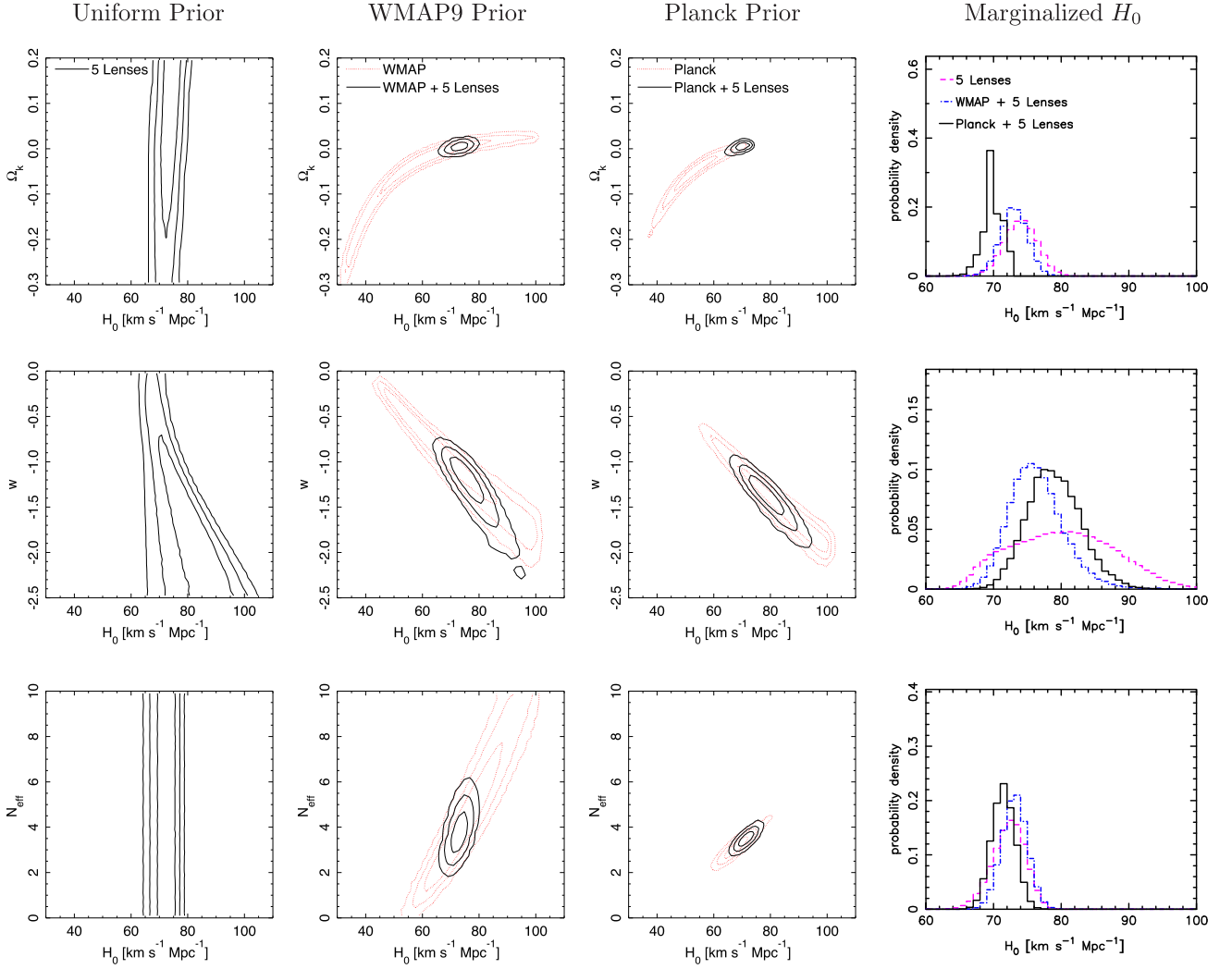
Figure 3. Forecasted cosmographic constraints from the H0LiCOW lens sample through measurements of $D_{\Delta t}$ and D_d. Columns from left to right are, respectively, the constraints from the H0LiCOW lenses alone (with uniform prior on cosmological parameters), lenses in combination with *WMAP* 9-yr results, lenses in combination with *Planck* 2015 results, and marginalized constraints on H_0 from the previous three columns. The H0LiCOW lenses primarily constrain H_0, which in turn break CMB parameter degeneracies to elucidate the spatial curvature of universe (Ω_k, top row), dark energy equation of state (w, middle row) and effective number of relativistic species (N_{eff}, bottom row). H0LiCOW lenses provide an independent, complementary and competitive probe of cosmology.

Table 5. Prior for 'uniform' cosmological models.

Cosmology	Prior ranges
Open ΛCDM	$H_0 \in [0, 120] \, \mathrm{km \, s^{-1} \, Mpc^{-1}}$
	$\Omega_m \in [0, 0.5]$
	$\Omega_\Lambda \in [0.5, 1]$
	$\Omega_k = 1 - \Omega_m - \Omega_\Lambda$
Flat wCDM	$H_0 \in [0, 120] \, \mathrm{km \, s^{-1} \, Mpc^{-1}}$
	$\Omega_m \in [0, 1]$
	$\Omega_{DE} = 1 - \Omega_m$
	$w \in [-2.5, 0]$
Flat $N_{eff}\Lambda$CDM	$H_0 \in [0, 120] \, \mathrm{km \, s^{-1} \, Mpc^{-1}}$
	$\Omega_m \in [0, 1]$
	$\Omega_\Lambda = 1 - \Omega_m$
	$N_{eff} \in [0, 10]$

chains have a prior with $H_0 < 100 \, \mathrm{km \, s^{-1} \, Mpc^{-1}}$ imposed. The cosmographic constraints of our lenses shown in Fig. 3 (from the forecasted measurements of $D_{\Delta t}$ and D_d) mostly stem from the $D_{\Delta t}$ measurements as a results of the substantially smaller uncertainties of $D_{\Delta t}$ than that of D_d. In fact, the cosmographic constraints from $D_{\Delta t}$ alone would increase the H_0 1σ uncertainties shown in Fig. 3 by at most $0.8 \, \mathrm{km \, s^{-1} \, Mpc^{-1}}$ (depending on the background cosmology). The additional cosmographic information from D_d would become more significant when the D_d uncertainties are reduced to $\sim$5–10 per cent (Jee et al. 2016).

As seen in the left column, the time-delay lenses primarily constrain H_0, and depend weakly (if at all) on other parameters. None the less, the time-delay distances $D_{\Delta t}$ and the lenses' angular diameter distances D_d provide some information on w, as the constraint contours are tilted rather than being vertical. With more lenses or smaller uncertainties on D_d measurements, the constraints on cosmology become more prominent (Jee et al. 2016). However, the

H0LiCOW lenses provide strong cosmographic constraints when combined with the CMB measurements since they help to break parameter degeneracies in the CMB. Thus, we should be able to place substantially better constraints on, for example, the spatial curvature, w and N_{eff} (middle two columns), compared to constraints from CMB alone. In particular, we expect better than 3.5 per cent precision on H_0 for the two cosmologies with $w = -1$ (open ΛCDM and flat $N_{eff}\Lambda$CDM)[9]; when w is allowed to vary, this constraint weakens to $\sim$11 per cent without CMB priors and $\sim$5 per cent with CMB priors in the wCDM cosmology, as visible in the rightmost panel in the middle row. By combining our five H0LiCOW lenses with *Planck*, we expect to achieve the following precisions: Ω_k to 0.004 in open ΛCDM, w to 0.14 in flat wCDM, and N_{eff} to 0.2 in flat $N_{eff}\Lambda$CDM (all 1σ uncertainties). These precisions are a factor of $\sim$15, $\sim$2, and $\sim$1.5, respectively, tighter than *Planck* on its own. Our H0LiCOW sample provides not only an independent check of systematics, but also a great complement to other cosmological probes for pinning down cosmological parameters.

7 SUMMARY AND OUTLOOK

We present the H0LiCOW program that aims to measure H_0 to <3.5 per cent in precision and accuracy (in most background cosmological models) with a sample of five time-delay lenses, completely independent of the cosmic distance ladder and other direct measurements of H_0. Our cosmographic information comes from measuring the distances to the lens systems, specifically $D_{\Delta t}$ and D_d.

To achieve our goal, we have obtained almost all the key ingredients for our lens sample[10]: (1) the time delays from the COSMOGRAIL and Very Large Array monitoring, (2) high-resolution *HST* imaging for modelling the lens mass distributions, (3) wide-field imaging and spectroscopy to quantify the effects of the lens environment, and (4) lens velocity dispersion measurements to augment our lensing mass models. Our new *HST* observations reveal Einstein rings in the lens systems that allow us to perform precision lens mass modelling.

The results of our recent blind analysis of HE 0435−1223 will appear in the companion H0LiCOW publications. H0LiCOW Paper II (Sluse et al. 2017) presents the spectroscopic campaign on the HE 0435−1223 field and identifies galaxy groups in the light cone containing the lens. H0LiCOW Paper III (Rusu et al. 2017) combines the spectroscopy, the wide-field imaging data, and the Millennium Simulation to derive the external convergence of the line-of-sight mass distributions. H0LiCOW Paper IV (Wong et al. 2017) models the lens mass distribution using the *HST* data, the time delays and the lens velocity dispersion to infer the time-delay distance, that is blinded throughout the analysis. H0LiCOW Paper V (Bonvin et al. 2017) presents the COSMOGRAIL monitoring of HE 0435−1223 and investigates the cosmological implications based on the three lenses (B1608+656, RXJ1131−1231and HE 0435−1223) that we have so far analysed.

With our sample of five lenses, we expect to measure H_0 to <3.5 per cent in precision and accuracy for the non-flat ΛCDM cosmology or flat $N_{eff}\Lambda$CDM cosmology, with $w = -1$. When w is allowed to vary, the constraint on H_0 degrades to $\sim$11 per cent with time-delay data only, and to $\sim$5 per cent when augmented with

CMB data. Our independent strong-lensing distances significantly improve cosmological constraints from the *Planck* data: the precisions on Ω_k, w, and N_{eff} improve by a factor of $\sim$15, $\sim$2, and 1.5, respectively, when we combine our lenses with *Planck*. Time-delay lenses are therefore highly complementary to other cosmological probes.

Our data set provides an excellent opportunity to study, in addition to cosmography, galaxy formation, and evolution. For example, we can study the distribution of dark matter in the lens galaxies by combining lensing and kinematics data, and also infer the stellar mass of the lens galaxies (e.g. Treu & Koopmans 2004; Barnabè et al. 2011; Sonnenfeld et al. 2012, 2015; Suyu et al. 2012b). By separately determining the stellar mass based on either (1) stellar population synthesis using multiband photometry (e.g. Auger et al. 2009; Treu et al. 2010; Oguri, Rusu & Falco 2014), or (2) identification/characterization of spectral features (e.g. van Dokkum & Conroy 2010; Conroy & van Dokkum 2012; Spiniello et al. 2012, 2014, 2015; Barnabè et al. 2013), and comparing this stellar mass to that obtained from lensing and dynamics, we can study properties of the stellar population and infer the stellar IMF slope (e.g. Grillo et al. 2009; Auger et al. 2010; Treu et al. 2010; Spiniello et al. 2011, 2015; Barnabè et al. 2013). There are about a dozen early-type lens galaxies that have been studied in detail for constraining the stellar IMF slope individually (e.g. Sonnenfeld et al. 2012; Barnabè et al. 2013; Spiniello et al. 2015; Newman et al. 2016), and these galaxies are all at redshifts below 0.35. Four of our H0LiCOW lens galaxies are at redshifts between 0.45 and 0.73, which would allow us to explore the stellar IMF with comparable precisions per lens galaxy as previous studies, but at substantially higher redshifts. Given the current tension in the IMF measurement between nearby ($z_d < 0.06$) lens galaxies and $z_d \sim 0.2$–0.3 lens galaxies (e.g. Smith & Lucey 2013; Newman et al. 2016), our H0LiCOW lenses would help assess whether the tensions are just limited to those particular objects or if they reflect a more general problem in our understanding of stellar populations. In addition, our lenses are natural telescopes that magnify the background sources, allowing us to study the host galaxies of the AGNs in detail and probe the origin of the co-evolution between supermassive black holes and their host galaxies (Peng et al. 2006; Rusu et al. 2016; Ding et al. 2017).

Our H0LiCOW program aims to establish gravitational lens time delays as an independent and competitive probe of cosmology, and paves the way for determining H_0 to 1 per cent in the future. Given the hundreds, if not thousands, of time-delay lens systems that are expected to be discovered in ongoing and future surveys such as the Sloan Digital Sky Survey (e.g. Oguri et al. 2006; Inada et al. 2012; More et al. 2016a), the Dark Energy Survey (e.g. Agnello et al. 2015), the Hyper Suprime-Cam Survey (e.g. Chan et al. 2016), the Kilo-Degree Survey (e.g. Napolitano et al. 2015), Euclid and the Large Synoptic Survey Telescope (Oguri & Marshall 2010), and continuous advances in high-resolution imaging and spectroscopy in the current and next generation of telescopes for observational follow-up (Linder 2015; Meng et al. 2015), the H0LiCOW program will provide the basis for extracting cosmological information from the wealth of strong-lensing data sets. In particular, we expect the combination of facilities at different wavelengths such as the *HST* in the optical/near-IR, *James Webb Space Telescope* in the IR, large and extremely large telescopes with adaptive optics, the Atacama Large Millimeter/submillimeter Array in the submillimetre waveband, and the Square Kilometre Array in the radio, will be of great synergistic value for studying these fruitful lenses.

---

[9] Relative to $H_0 = 72 \, \mathrm{km \, s^{-1} \, Mpc^{-1}}$.
[10] With spectroscopic observations of HE 1104−1805 pending for lens velocity dispersion measurement.

REFERENCES

Agnello A. et al., 2015, MNRAS, 454, 1260
Anderson L. et al., 2014, MNRAS, 441, 24
Appenzeller I. et al., 1998, The Messenger, 94, 1
Aubourg É. et al., 2015, Phys. Rev. D, 92, 123516
Auger M. W., Treu T., Bolton A. S., Gavazzi R., Koopmans L. V. E., Marshall P. J., Bundy K., Moustakas L. A., 2009, ApJ, 705, 1099
Auger M. W., Treu T., Bolton A. S., Gavazzi R., Koopmans L. V. E., Marshall P. J., Moustakas L. A., Burles S., 2010, ApJ, 724, 511
Bacon R. et al., 2012, The Messenger, 147, 4
Barnabè M., Czoske O., Koopmans L. V. E., Treu T., Bolton A. S., Gavazzi R., 2009, MNRAS, 399, 21
Barnabè M., Czoske O., Koopmans L. V. E., Treu T., Bolton A. S., 2011, MNRAS, 415, 2215

Barnabè M., Spiniello C., Koopmans L. V. E., Trager S. C., Czoske O., Treu T., 2013, MNRAS, 436, 253

Beaton R. L. et al., 2016, ApJ, 832, 210

Betoule M. et al., 2014, A&A, 568, A22

Birrer S., Amara A., Refregier A., 2015, ApJ, 813, 102

Birrer S., Amara A., Refregier A., 2016, JCAP, 08, 020

Blake C. et al., 2011, MNRAS, 415, 2892

Blandford R. D., Kochanek C. S., 2004, in Bahcall J. et al., eds, Gravitational Lenses. World Scientific Press, Singapore, p. 103

Blandford R., Narayan R., 1986, ApJ, 310, 568

Bonvin V., Tewes M., Courbin F., Kuntzer T., Sluse D., Meylan G., 2016, A&A, 585, A88

Bonvin V. et al., 2017, MNRAS 465, 4914 (H0LiCOW Paper V)

Boulade O. et al., 2003, in Iye M., Moorwood A. F. M., eds, Proc. SPIEVol. 4841, Instrument Design and Performance for Optical/Infrared Ground-based Telescopes. SPIE, Bellingham, p. 72

Browne I. W. A. et al., 2003, MNRAS, 341, 13

Burud I. et al., 2002, A&A, 383, 71

Cantale N., Courbin F., Tewes M., Jablonka. P., Meylan G., 2016, A&A, 589, A81

Casali M. et al., 2006, in McLean I. S., Iye M., eds, Proc. SPIEConf. Ser. Vol. 6269, Ground-based and Airborne Instrumentation for Astronomy. SPIE, Bellingham, p. 62690W

Chan J. H. H. et al., 2016, ApJ, 832, 135

Chen G. C. F. et al., 2016, MNRAS, 462, 3457

Claeskens J.-F., Sluse D., Riaud P., Surdej J., 2006, A&A, 451, 865

Collett T. E., Cunnington S. D., 2016, MNRAS, 462, 3255

Collett T. E. et al., 2013, MNRAS, 432, 679

Conley A. et al., 2006, ApJ, 644, 1

Conley A. et al., 2011, ApJS, 192, 1

Conroy C., van Dokkum P. G., 2012, ApJ, 760, 71

Courbin F., Lidman C., Magain P., 1998, A&A, 330, 57

Courbin F., Eigenbrod A., Vuissoz C., Meylan G., Magain P., 2005, in Mellier Y., Meylan G., eds, Proc. IAU Symp. 225, Gravitational Lensing Impact on Cosmology. Cambridge Univ. Press, Cambridge, p. 297

Courbin F. et al., 2011, A&A, 536, A53

Dark Energy Survey Collaboration, Diehl T., 2012, Phys. Procedia, 37, 1332

Ding X. et al., 2017, MNRAS, 465, 4634

Dobler G., Fassnacht C. D., Treu T., Marshall P., Liao K., Hojjati A., Linder E., Rumbaugh N., 2015, ApJ, 799, 168

Dye S., Evans N. W., Belokurov V., Warren S. J., Hewett P., 2008, MNRAS, 388, 384

Eigenbrod A., Courbin F., Meylan G., Vuissoz C., Magain P., 2006, A&A, 451, 759

Eisenstein D. J. et al., 2005, ApJ, 633, 560

Falco E. E., Gorenstein M. V., Shapiro I. I., 1985, ApJ, 289, L1

Fassnacht C. D., Womble D. S., Neugebauer G., Browne I. W. A., Readhead A. C. S., Matthews K., Pearson T. J., 1996, ApJ, 460, L103

Fassnacht C. D., Pearson T. J., Readhead A. C. S., Browne I. W. A., Koopmans L. V. E., Myers S. T., Wilkinson P. N., 1999, ApJ, 527, 498

Fassnacht C. D., Xanthopoulos E., Koopmans L. V. E., Rusin D., 2002, ApJ, 581, 823

Fassnacht C. D., Gal R. R., Lubin L. M., McKean J. P., Squires G. K., Readhead A. C. S., 2006, ApJ, 642, 30

Fassnacht C. D., Koopmans L. V. E., Wong K. C., 2011, MNRAS, 410, 2167

Fazio G. G. et al., 2004, ApJS, 154, 10

Freedman W. L., Madore B. F., Scowcroft V., Burns C., Monson A., Persson S. E., Seibert M., Rigby J., 2012, ApJ, 758, 24

Futamase T., Hamana T., 1999, Prog. Theor. Phys., 102, 1037

Futamase T., Yoshida S., 2001, Prog. Theor. Phys., 105, 887

Gao F. et al., 2016, ApJ, 817, 128

Goobar A. et al., 2016, preprint (arXiv:1611.00014)

Greene Z. S. et al., 2013, ApJ, 768, 39

Grillo C., Lombardi M., Bertin G., 2008, A&A, 477, 397

Grillo C., Gobat R., Lombardi M., Rosati P., 2009, A&A, 501, 461

Grillo C. et al., 2016, ApJ, 822, 78

Harva M., Raychaudhury S., 2008, Neurocomputing, 72, 32

Heavens A., Jimenez R., Verde L., 2014, Phys. Rev. Lett., 113, 241302

Hewett P. C., Wild V., 2010, MNRAS, 405, 2302

Heymans C. et al., 2012, MNRAS, 427, 146

Hilbert S., White S. D. M., Hartlap J., Schneider P., 2007, MNRAS, 382, 121

Hilbert S., Hartlap J., White S. D. M., Schneider P., 2009, A&A, 499, 31

Hinshaw G. et al., 2013, ApJS, 208, 19

Hirv A., Olspert N., Pelt J., 2011, Balt. Astron., 20, 125

Hjorth J. et al., 2002, ApJ, 572, L11

Hodapp K. W. et al., 2003, PASP, 115, 1388

Hojjati A., Kim A. G., Linder E. V., 2013, Phys. Rev. D, 87, 123512

Holder G. P., Schechter P. L., 2003, ApJ, 589, 688

Hook I. M., Jørgensen I., Allington-Smith J. R., Davies R. L., Metcalfe N., Murowinski R. G., Crampton D., 2004, PASP, 116, 425

Hu W., 2005, in Wolff S. C., Lauer T. R., eds, ASP Conf. Ser. Vol. 339, Observing Dark Energy. Astron. Soc. Pac., San Francisco, p. 215

Ichikawa T. et al., 2006, in McLean I. S., Iye M., eds, Proc. SPIEConf. Ser. Vol. 6269, Ground-based and Airborne Instrumentation for Astronomy. SPIE, Bellingham, p. 626916

Inada N. et al., 2012, AJ, 143, 119

Jee I., Komatsu E., Suyu S. H., 2015, J. Cosmology Astropart. Phys., 11, 033

Jee I., Komatsu E., Suyu S. H., Huterer D., 2016, J. Cosmology Astropart. Phys., 2016, 031

Kawamata R., Oguri M., Ishigaki M., Shimasaku K., Ouchi M., 2016, ApJ, 819, 114

Kazin E. A. et al., 2014, MNRAS, 441, 3524

Kelly P. L. et al., 2015, Science, 347, 1123

Kelly P. L. et al., 2016, ApJ, 819, L8

Kissler-Patig M. et al., 2008, A&A, 491, 941

Kochanek C. S., 2002, ApJ, 578, 25

Kochanek C. S., Keeton C. R., McLeod B. A., 2001, ApJ, 547, 50

Kochanek C. S., Morgan N. D., Falco E. E., McLeod B. A., Winn J. N., Dembicky J., Ketzeback B., 2006, ApJ, 640, 47

Komatsu E. et al., 2011, ApJS, 192, 18

Koopmans L. V. E., 2005, MNRAS, 363, 1136

Koopmans L. V. E., Treu T., Fassnacht C. D., Blandford R. D., Surpi G., 2003, ApJ, 599, 70

Kuo C. Y. et al., 2015, ApJ, 800, 26

Larkin J. et al., 2006, in McLean I. S., Iye M., eds, Proc. SPIEConf. Ser. Vol. 6269, Ground-based and Airborne Instrumentation for Astronomy. SPIE, Bellingham, p. 62691A

Liao K. et al., 2015, ApJ, 800, 11

Lidman C., Courbin F., Kneib J.-P., Golse G., Castander F., Soucail G., 2000, A&A, 364, L62

Linder E. V., 2015, Phys. Rev. D, 91, 083511

McCully C., Keeton C. R., Wong K. C., Zabludoff A. I., 2014, MNRAS, 443, 3631

McCully C., Keeton C. R., Wong K. C., Zabludoff A. I., 2016, ApJ, 836, 141

Magain P., Courbin F., Sohy S., 1998, ApJ, 494, 472

Meng X.-L., Treu T., Agnello A., Auger M. W., Liao K., Marshall P. J., 2015, J. Cosmology Astropart. Phys., 9, 059

Miyazaki S. et al., 2002, PASJ, 54, 833

Momcheva I., Williams K., Keeton C., Zabludoff A., 2006, ApJ, 641, 169

Momcheva I. G., Williams K. A., Cool R. J., Keeton C. R., Zabludoff A. I., 2015, ApJS, 219, 29

More A. et al., 2016a, MNRAS, 456, 1595

More A., Suyu S. H., Oguri M., More S., Lee C.-H., 2016b, ApJ, 835, L25

Morgan N. D., Caldwell J. A. R., Schechter P. L., Dressler A., Egami E., Rix H.-W., 2004, AJ, 127, 2617

Morgan N. D., Kochanek C. S., Pevunova O., Schechter P. L., 2005, AJ, 129, 2531

Morgan C. W., Eyler M. E., Kochanek C. S., Morgan N. D., Falco E. E., Vuissoz C., Courbin F., Meylan G., 2008, ApJ, 676, 80

Myers S. T. et al., 1995, ApJ, 447, L5

Myers S. T. et al., 2003, MNRAS, 341, 1

Napolitano N. R. et al., 2015, The Universe of Digital Sky Surveys. Springer-Verlag, Berlin

Newman A. B., Smith R. J., Conroy C., Villaume A., van Dokkum P., 2016, ApJ, preprint (arXiv:1612.00065)

Ofek E. O., Maoz D., Rix H.-W., Kochanek C. S., Falco E. E., 2006, ApJ, 641, 70

Oguri M., Marshall P. J., 2010, MNRAS, 405, 2579

Oguri M. et al., 2006, AJ, 132, 999

Oguri M., Rusu C. E., Falco E. E., 2014, MNRAS, 439, 2494

Oke J. B. et al., 1995, PASP, 107, 375

Paraficz D., Hjorth J., 2009, A&A, 507, L49

Pelt J., Kayser R., Refsdal S., Schramm T., 1996, A&A, 305, 97

Peng C. Y., Impey C. D., Rix H.-W., Kochanek C. S., Keeton C. R., Falco E. E., Lehár J., McLeod B. A., 2006, ApJ, 649, 616

Percival W. J. et al., 2010, MNRAS, 401, 2148

Perlmutter S. et al., 1999, ApJ, 517, 565

Pirard J.-F. et al., 2004, in Moorwood A. F. M., Iye M., eds, Proc. SPIEConf. Ser. Vol. 5492, Ground-based Instrumentation for Astronomy. SPIE, Bellingham, p. 1763

Planck Collaboration XVI, 2014, A&A, 571, A16

Planck Collaboration XIII, 2016, A&A, 594, A13

Poindexter S., Morgan N., Kochanek C. S., Falco E. E., 2007, ApJ, 660, 146

Press W. H., Rybicki G. B., Hewitt J. N., 1992, ApJ, 385, 404

Quimby R. M. et al., 2014, Science, 344, 396

Refsdal S., 1964, MNRAS, 128, 307

Reid M. J., Braatz J. A., Condon J. J., Lo K. Y., Kuo C. Y., Impellizzeri C. M. V., Henkel C., 2013, ApJ, 767, 154

Remy M., Claeskens J.-F., Surdej J., Hjorth J., Refsdal S., Wucknitz O., Sørensen A. N., Grundahl F., 1998, New Astron., 3, 379

Riess A. G. et al., 1998, AJ, 116, 1009

Riess A. G. et al., 2016, ApJ, 826, 56

Rockosi C. et al., 2010, in McLean I. S., Ramsay S. K., Takami H., eds, Ground-based and Airborne Instrumentation for Astronomy III. SPIE, Bellingham, p. 77350R

Romanowsky A. J., Kochanek C. S., 1999, ApJ, 516, 18

Ross A. J., Samushia L., Howlett C., Percival W. J., Burden A., Manera M., 2015, MNRAS, 449, 835

Rumbaugh N., Fassnacht C. D., McKean J. P., Koopmans L. V. E., Auger M. W., Suyu S. H., 2015, MNRAS, 450, 1042

Rusu C. E. et al., 2016, MNRAS, 458, 2

Rusu C. E. et al., 2017, preprint (arXiv:1607.01047) (H0LiCOW Paper III)

Schechter P. L. et al., 1997, ApJ, 475, L85

Schneider P., Sluse D., 2013, A&A, 559, A37

Schneider P., Sluse D., 2014, A&A, 564, A103

Schneider P., Ehlers J., Falco E. E., 1992, Gravitational Lenses, XIV. Springer-Verlag, Berlin

Sheinis A. I., Bolte M., Epps H. W., Kibrick R. I., Miller J. S., Radovan M. V., Bigelow B. C., Sutin B. M., 2002, PASP, 114, 851

Sluse D., Tewes M., 2014, A&A, 571, A60

Sluse D. et al., 2003, A&A, 406, L43

Sluse D., Claeskens J.-F., Hutsemékers D., Surdej J., 2007, A&A, 468, 885

Sluse D., Hutsemékers D., Courbin F., Meylan G., Wambsganss J., 2012, A&A, 544, A62

Sluse D. et al., 2017, MNRAS, preprint (arXiv:1607.00382) (H0LiCOW Paper II)

Smette A., Robertson J. G., Shaver P. A., Reimers D., Wisotzki L., Koehler T., 1995, A&AS, 113, 199

Smith R. J., Lucey J. R., 2013, MNRAS, 434, 1964

Sonnenfeld A., Treu T., Gavazzi R., Marshall P. J., Auger M. W., Suyu S. H., Koopmans L. V. E., Bolton A. S., 2012, ApJ, 752, 163

Sonnenfeld A., Treu T., Marshall P. J., Suyu S. H., Gavazzi R., Auger M. W., Nipoti C., 2015, ApJ, 800, 94

Spiniello C., Koopmans L. V. E., Trager S. C., Czoske O., Treu T., 2011, MNRAS, 417, 3000

Spiniello C., Trager S. C., Koopmans L. V. E., Chen Y. P., 2012, ApJ, 753, L32

Spiniello C., Trager S., Koopmans L. V. E., Conroy C., 2014, MNRAS, 438, 1483

Spiniello C., Barnabè M., Koopmans L. V. E., Trager S. C., 2015, MNRAS, 452, L21

Surpi G., Blandford R. D., 2003, ApJ, 584, 100

Suyu S. H., 2012, MNRAS, 426, 868

Suyu S. H., Halkola A., 2010, A&A, 524, A94

Suyu S. H., Marshall P. J., Blandford R. D., Fassnacht C. D., Koopmans L. V. E., McKean J. P., Treu T., 2009, ApJ, 691, 277

Suyu S. H., Marshall P. J., Auger M. W., Hilbert S., Blandford R. D., Koopmans L. V. E., Fassnacht C. D., Treu T., 2010, ApJ, 711, 201

Suyu S. H. et al., 2012a, preprint (arXiv:1202.4459)

Suyu S. H. et al., 2012b, ApJ, 750, 10

Suyu S. H. et al., 2013, ApJ, 766, 70

Suyu S. H. et al., 2014, ApJ, 788, L35

Suzuki R. et al., 2008, PASJ, 60, 1347

Suzuki N. et al., 2012, ApJ, 746, 85

Tewes M., Courbin F., Meylan G., 2013a, A&A, 553, A120

Tewes M. et al., 2013b, A&A, 556, A22

Treu T., Koopmans L. V. E., 2002, MNRAS, 337, L6

Treu T., Koopmans L. V. E., 2004, ApJ, 611, 739

Treu T., Marshall P. J., 2016, A&AR, 24, 11

Treu T., Gavazzi R., Gorecki A., Marshall P. J., Koopmans L. V. E., Bolton A. S., Moustakas L. A., Burles S., 2009, ApJ, 690, 670

Treu T., Auger M. W., Koopmans L. V. E., Gavazzi R., Marshall P. J., Bolton A. S., 2010, ApJ, 709, 1195

Treu T. et al., 2016, ApJ, 817, 60

Unruh S., Schneider P., Sluse D., 2016, A&A, preprint (arXiv:1606.04321)

van Dokkum P. G., Conroy C., 2010, Nature, 468, 940

Vanderriest C., Schneider J., Herpe G., Chevreton M., Moles M., Wlerick G., 1989, A&A, 215, 1

Vegetti S., Koopmans L. V. E., 2009, MNRAS, 392, 945

Vernet J. et al., 2011, A&A, 536, A105

von der Linden A. et al., 2014, MNRAS, 439, 2

Vuissoz C. et al., 2007, A&A, 464, 845

Vuissoz C. et al., 2008, A&A, 488, 481

Walsh D., Carswell R. F., Weymann R. J., 1979, Nature, 279, 381

Warren S. J., Dye S., 2003, ApJ, 590, 673

Weinberg D. H., Mortonson M. J., Eisenstein D. J., Hirata C., Riess A. G., Rozo E., 2013, Phys. Rep., 530, 87

Williams K. A., Momcheva I., Keeton C. R., Zabludoff A. I., Lehár J., 2006, ApJ, 646, 85

Wisotzki L., Koehler T., Kayser R., Reimers D., 1993, A&A, 278, L15

Wisotzki L., Christlieb N., Bade N., Beckmann V., Köhler T., Vanelle C., Reimers D., 2000, A&A, 358, 77

Wisotzki L., Schechter P. L., Bradt H. V., Heinmüller J., Reimers D., 2002, A&A, 395, 17

Wong K. C. et al., 2017, MNRAS, 465, 4895 (H0LiCOW Paper IV)

Wucknitz O., 2002, MNRAS, 332, 951

Wucknitz O., Biggs A. D., Browne I. W. A., 2004, MNRAS, 349, 14

Xu D., Sluse D., Schneider P., Springel V., Vogelsberger M., Nelson D., Hernquist L., 2016, MNRAS, 456, 739

[1]*Max-Planck-Institut für Astrophysik, Karl-Schwarzschild-Str. 1, D-85748 Garching, Germany*

[2]*Institute of Astronomy and Astrophysics, Academia Sinica, PO Box 23-141, Taipei 10617, Taiwan*

[3]*Physik-Department, Technische Universität München, James-Franck-Straße 1, D-85748 Garching, Germany*

[4]*Laboratoire d'Astrophysique, Ecole Polytechnique Fédérale de Lausanne (EPFL), Observatoire de Sauverny, CH-1290 Versoix, Switzerland*

[5]*Department of Physics, University of California, Davis, CA 95616, USA*

[6]*STAR Institute, Quartier Agora – Allée du six Août, 19c B-4000 Liège, Belgium*

[7]*Department of Physics and Astronomy, University of California, Los Angeles, CA 90095, USA*

[8]*National Astronomical Observatory of Japan, 2-21-1 Osawa, Mitaka, Tokyo 181-8588, Japan*

[9]*Institute of Astronomy, University of Cambridge, Madingley Road, Cambridge CB3 0HA, UK*

[10]*Department of Astronomy, Beijing Normal University, Beijing 100875, China*

[11]*Exzellenzcluster Universe, Boltzmannstr. 2, D-85748 Garching, Germany*

[12]*Ludwig-Maximilians-Universität, Universitäts-Sternwarte, Scheinerstr. 1, D-81679 München, Germany*

[13]*Kavli Institute for Particle Astrophysics and Cosmology, Stanford University, 452 Lomita Mall, Stanford, CA 94035, USA*

[14]*Kavli IPMU (WPI), UTIAS, The University of Tokyo, Kashiwa, Chiba 277-8583, Japan*

[15]*Physics Department, University of California, Santa Barbara, CA 93106, USA*

[16]*Argelander-Institut für Astronomie, Auf dem Hügel 71, D-53121 Bonn, Germany*

[17]*ESO – European Southern Observatory, D-85748 Garching bei München, Germany*

[18]*Institute of Cosmology and Gravitation, University of Portsmouth, Burnaby Rd, Portsmouth PO1 3FX, UK*

[19]*Kapteyn Astronomical Institute, University of Groningen, PO Box 800, NL-9700 AV Groningen, the Netherlands*

This paper has been typeset from a TEX/LATEX file prepared by the author.